Negative refraction of longitudinal waves in a two-dimensional solid-solid phononic crystal

C. Croënne,[1,3] E. D. Manga,[2,3,4] B. Morvan,[2,3] A. Tinel,[2,3] B. Dubus,[1,3] J. Vasseur,[1,3] and A.-C. Hladky-Hennion[1,3]

[1]*Institut d'Électronique, de Microélectronique et de Nanotechnologie, UMR-8520 CNRS, 41 boulevard Vauban, F-59046 Lille, France*

[2]*Laboratoire Ondes et Milieux Complexes, FRE-3102 CNRS, Groupe Ondes Acoustiques, Université du Havre, Place Robert Schuman, BP 4006, F-76610 Le Havre, France*

[3]*Fédération Acoustique du Nord-Ouest, FR 3110 CNRS, Place Robert Schuman, F-76610 Le Havre, France*

[4]*Laboratoire Imagerie et Cerveau, UMR-U 930, Équipe Caractérisation Ultrasonore et Piézoélectricité, Université François Rabelais de Tours, Rue de la Chocolaterie, BP 3140, F-41034 Blois, France*

(Received 26 October 2010; revised manuscript received 10 January 2011; published 25 February 2011)

Negative refraction of longitudinal waves is evidenced experimentally in a two-dimensional phononic crystal (PC) with a solid matrix. The PC is made of a triangular arrangement of steel rods embedded in epoxy. The dispersion curves present a branch with a negative slope, corresponding to a mixed mode with a predominantly longitudinal behavior. Experiments are carried out on a prism-shaped PC inserted inside an epoxy block, and excited with a longitudinal transducer. Measurement of the refraction angle at the output side of the PC shows the negative refraction of longitudinal waves through a solid PC. Theoretical results agree quite well with the experimental results. The possibility to use the PC in a fluid background is verified numerically, with the simulation of a focusing flat lens.

DOI: 10.1103/PhysRevB.83.054301 PACS number(s): 43.20.+g, 43.35.+d, 43.40.+s, 63.20.−e

I. INTRODUCTION

Phononic crystals (PCs) are usually defined as artificial materials made of periodic distributions of scatterers embedded in a matrix. By varying the geometry of the array of inclusions and the nature of the constitutive materials, the band structures of PCs may present absolute stop bands under certain conditions. Owing to this property, PCs were first proposed for realizing sonic insulators or for designing efficient filters for elastic waves.[1] Moreover, band structures of PCs may exhibit dispersion curves with a negative slope, i.e., the wave vector and the group-velocity vector associated with an acoustic wave point in opposite directions. This property is typical of a left-handed material and implies a negative index of refraction in the Snell-Descartes law, even though it should be noted that negative angles of refraction can be obtained also in strongly anisotropic positive-index PCs.[2–7] Using negative-index PCs, flat superlenses able to focus elastic waves with a resolution lower than the diffraction limit have been realized.[8] Such superlenses have potential applications in the fields of medical imaging or ultrasonic beam-based therapy. Numerous papers were first devoted to the negative refraction of acoustic waves in PCs made of arrays of solid cylinders immersed in a fluid (gas or liquid).[9–14] More specifically, Sukhovich *et al*. showed experimentally and theoretically that super resolution can be achieved by using a PC lens made of a triangular array of steel cylinders immersed in methanol and surrounded with water.[15] Nevertheless, from a practical point of view, it is more appropriate to consider a PC slab made with a solid matrix. While only longitudinal waves may propagate in fluid matrix PCs, longitudinal and transverse waves are coupled together in solid matrix PCs. Studying the optimum conditions for negative refraction is a much more complicated topic. With the help of the multiple scattering method, Li *et al*.[16] studied numerically the negative refraction imaging effect of longitudinal and transverse-elastic waves by two-dimensional (2D) three-component PCs. In a recent paper, Morvan *et al*.[17] have shown theoretically and experimentally that the negative refraction of an elastic wave with a predominantly transverse polarization may occur in a square array of holes drilled in an aluminum block. Other authors have also demonstrated numerically that a similar type of crystal can be used to build a focusing flat lens.[18] In the present paper, we focus on the occurrence of negative refraction of an elastic wave with a predominantly longitudinal behavior in a 2D PC made of steel cylinders embedded in an epoxy resin matrix. Owing to its longitudinal polarization, the negatively refracted wave can be easily excited by an incident longitudinal wave launched from a surrounding fluid medium, which is a key point for some applications such as imaging of biological media.

First, the dispersion curves of the PC made of a triangular array of steel rods embedded in an epoxy matrix are presented. Then, an experimental work is devoted to a prism-shaped PC located inside an epoxy block, excited by a longitudinal transducer. The displacements at the opposite face of the sample are picked up using a laser vibrometer. The signals are analyzed in the Fourier domain (wave number, frequency) and show a clear negative refraction of longitudinal waves, consistent with the theoretical results. Finally, the behavior of the PC in a fluid environment is verified numerically with the simulation of a focusing flat lens.

II. NUMERICAL ANALYSIS: PRISM IN A SOLID ENVIRONMENT

The PC considered is made of a triangular arrangement of steel rods embedded in an epoxy matrix. The diameter of the steel rods is equal to 2 mm, and the lattice parameter is 2.84 mm. Thus, the filling factor of steel rods in the epoxy matrix is equal to 0.45. The density of steel is 7800 kg/m^{3}and the longitudinal and transverse wave velocities are $V_{L,s} = 6180$ m/s and $V_{T,s} = 3245$ m/s respectively. For the epoxy, the density is 1150 kg/m^3; the longitudinal and transverse wave velocities

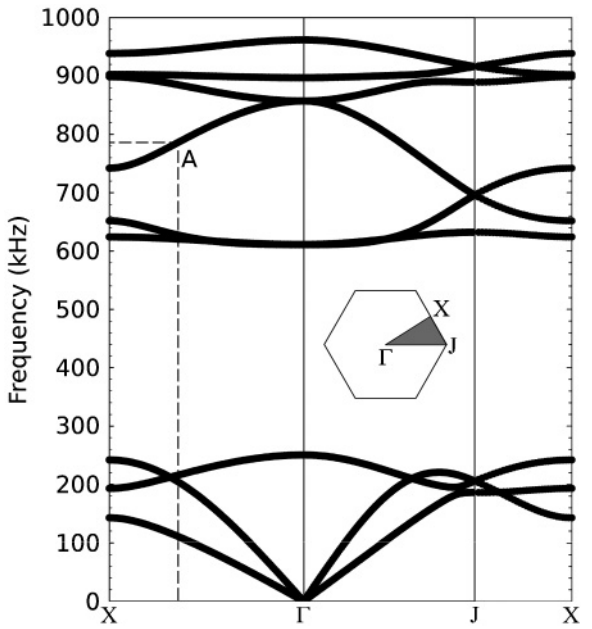

FIG. 1. Elastic band structure for the 2D PC made of a triangular array of steel rods in an epoxy matrix.

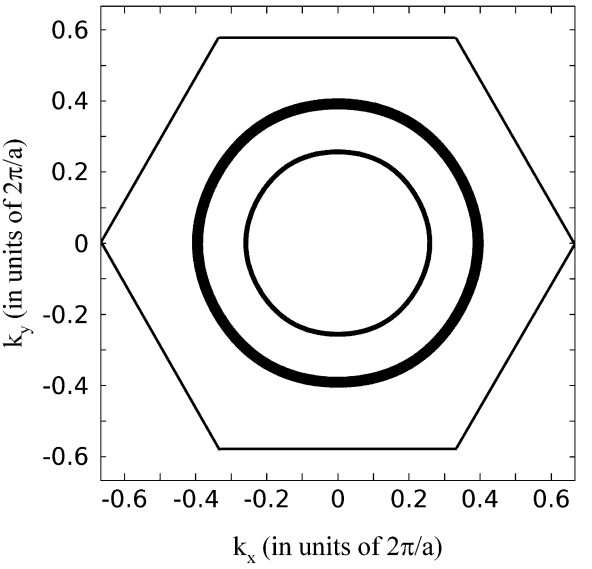

FIG. 3. EFCs of the PC at 780 kHz (thick line) and 820 kHz (thin line).

are $V_{L,e} = 2440$ m/s and $V_{T,e} = 1130$ m/s, respectively. In the frequency range of interest, epoxy is a viscous medium and attenuation takes place. It has been measured in bulk epoxy for the longitudinal waves, which exhibit an exponential decrease of displacement modulus with the distance x, $\exp(-ax)$, where $\alpha = 39$ m^{-1}. This corresponds to a loss tangent of $\sim$3.6% for the Young's modulus of the epoxy. Still, owing to limitations in the finite-element method code employed here,[19] losses in the epoxy matrix must be neglected in the calculation of the dispersion curves.

Figure 1 displays those dispersion curves in the first Brillouin zone, on the ΓJX path (see inset). It shows the variations of the frequency (in kHz) versus the reduced wave number. The figure exhibits several branches: The first two branches are issued from the Γ point and correspond to quasitransverse and quasilongitudinal waves. In the upper part of the dispersion curve, a branch with a negative slope is observed along the ΓX direction and is studied in this paper. In this frequency range (750 kHz, 860 kHz), the phase velocity and the group velocity have opposite signs. Figure 2 presents the displacement field at $k = 870$ rad m^{-1} and $F = 786$ kHz, denoted by point A in Fig. 1. It can be seen that, for a direction of propagation along x (i.e., ΓX direction), the displacement fields along x and y are, respectively, even and odd functions of y, which means that the mode under study is symmetric. Additionally, the displacement values show that it has a predominantly longitudinal behavior. Calculations show that, by varying the spacing between the cylinders, the frequency band where a unique branch with a negative slope for the longitudinal wave is obtained reaches its maximum width when the filling factor is 0.45. Figure 3 presents the equifrequency contours (EFCs) at 780 and 820 kHz, i.e., the intersection of the three-dimensional (3D) dispersion curves with a horizontal plane, corresponding to a fixed frequency. They exhibit a circular shape in the frequency range of interest. Therefore, the wave vector of the elastic wave and the group velocity are antiparallel, whatever the propagation direction. The radius of the EFC clearly decreases as the frequency increases, as expected for left-handed materials. The group velocity ($d\omega/dk$) can be calculated from Fig. 1: It varies between 350 and 940 m/s in the frequency range of interest. The phase velocity in the PC V_{PC}, determined by the ratio ω/k, presents large variations, from 3000 m/s at 750 kHz to 24 000 m/s at 860 kHz.

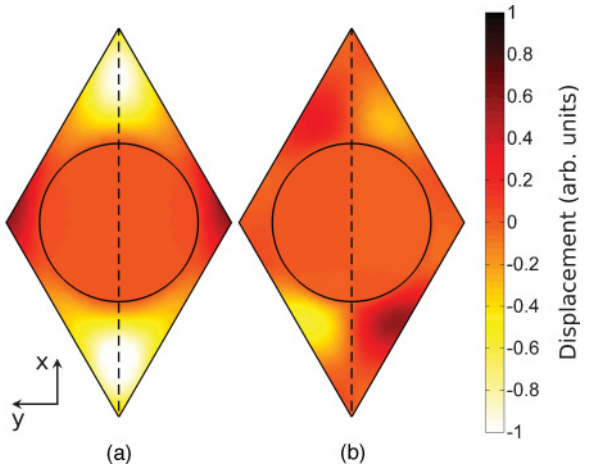

FIG. 2. (Color online) Displacement field on point A in Fig. 1 ($k_{PC} = 870$ rad m^{-1}, $F = 786$ kHz) inside the unit cell of an infinite crystal, along directions (a) x and (b) y. Propagation direction is along x.

III. EXPERIMENTAL RESULTS

A schematic description of the sample is presented in Fig. 4. The prism-shaped PC is located in a parallelepipedic block (105 mm $\times$ 69 mm $\times$ 60 mm). The PC is fabricated as

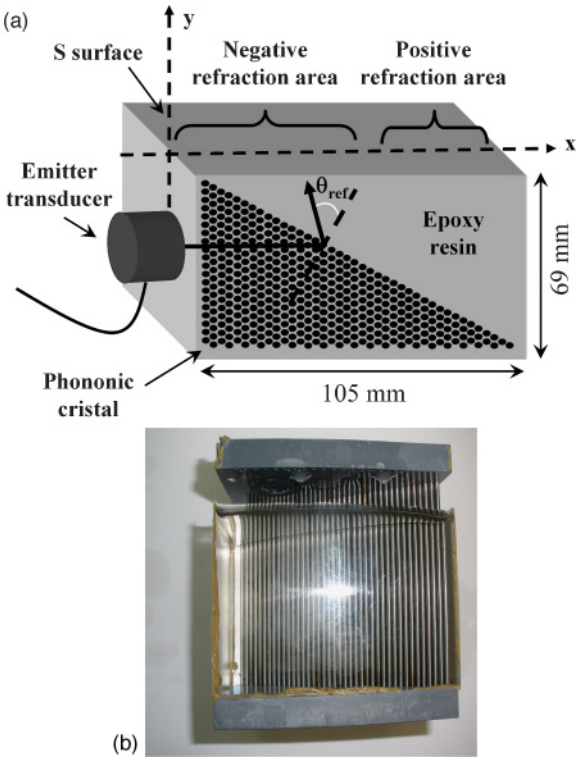

FIG. 4. (Color online) (a) Schematic description of the experimental setup and (b) view of the fabricated steel-epoxy PC.

follows. First, the steel rods are placed upon a triangular periodic arrangement between two drilled plates in order to obtain a prism-shaped PC: 40 rods for the base and 20 rods for the height, constituting a rectangular triangle, containing a total number of 420 rods. The two other angles of the prism are respectively equal to 30° and 60°. Second, the prismatic arrangement of rods is embedded in the liquid epoxy resin. A partial vacuum is used during the hardening of the resin (∼24 h) in order to avoid residual air bubbles in the PC. It should be noted that, with this fabrication process, both the PC prism (steel rods in epoxy) and its environment (bulk epoxy) are built simultaneously as a single block, which facilitates their coupling.

A large frequency band (320–800 kHz) piezoelectric transducer is used in order to generate a longitudinal wave along the x direction. Its diameter is equal to 2.54 cm, corresponding to approximately nine periods of the PC. The distance between the transducer and the input side of the PC is 1.5 mm. A burst of ten periods and 30 V amplitude at 780 kHz is used for the excitation. Because the source is large with respect to the wavelength in epoxy (∼8 × the longitudinal wavelength at 780 kHz), most of the energy impinges the crystal under normal incidence. Therefore, the refraction angle at the first interface is zero, and a longitudinal wave propagates through the PC along the ΓX direction. It reaches the second interface of the PC with a 60° angle, with respect to the normal to the interface. Then, it is refracted in the bulk epoxy medium. Because the incidence is oblique with respect to the prism interface, the single longitudinal mode inside the PC can couple with both a longitudinal and a transverse wave in the surrounding bulk epoxy. The corresponding refraction angles

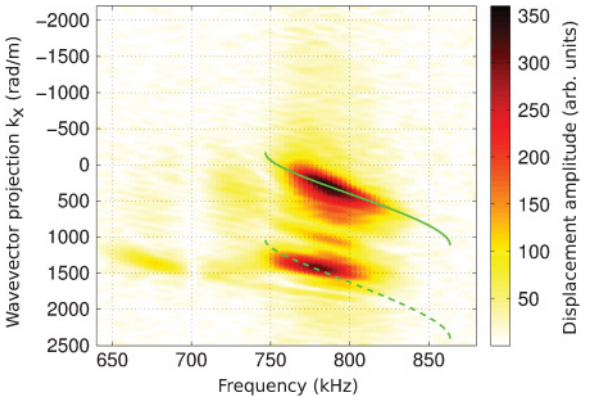

FIG. 5. (Color online) Amplitude (in arbitrary units) of the measured displacement along the y direction on the top surface in the (k_x, F) space. The solid and dashed curves show the theoretical values of the wave-vector projection on the x axis for the longitudinal and transverse refracted waves, respectively.

are noted as $\theta_{L,\mathrm{ref}}$ and $\theta_{T,\mathrm{ref}}$, respectively. For clarity, a clockwise convention is used for all angles, so that negative angles are obtained for negative refraction. Then the waves reach the upper surface S of the sample with angles equal to $\theta_{L,\mathrm{ref}} + 30°$ and $\theta_{T,\mathrm{ref}} + 30°$, respectively, with respect to the surface normal.

A Polytec® laser vibrometer is used to detect the normal (y direction) surface displacements on the upper surface S. A signal is observed in the area where a negatively refracted wave is expected. Values of k_x, an in-plane component of the wave vector to the surface S, are obtained by performing a time and spatial Fourier transform on time-space signals.[20] This diagram (Fig. 5) presents two main spots. Using the Snell-Descartes law, the wave-vector values inside the crystal extracted from the band diagram (Fig. 1) and the wave-vector values in epoxy for longitudinal and transverse waves, the theoretical $\theta_{L,\mathrm{ref}}(F)$ and $\theta_{T,\mathrm{ref}}(F)$ curves can be deduced, respectively, and therefore the theoretical curves,

$$k_{i,x}(F) = (2\pi F V_{i,e}) \sin(\theta_{i,\mathrm{ref}} + 30°), \qquad (1)$$

with i being L or T for longitudinal and transverse waves, respectively, can be drawn on Fig. 5. The superposition of the curves and the diagram suggests that the two main spots of the Fourier transform correspond to the transverse and longitudinal beams refracted at the PC exit interface. Only the longitudinal spot is under study here because it corresponds to the wave that can be coupled to an external fluid medium. Following the maximum ridge of this spot, the experimental $k_{L,x}(F)$ curve is collected and the refraction angles are then deduced using Eq. (1). The resulting refraction angles, presented in Fig. 6 as a function of the frequency, are clearly negative with respect to the normal to the exit interface of the PC. Experimental angles are compared to the theoretical angles previously deduced. Theoretical and experimental results are in good agreement in a broad frequency range, even though losses were not taken into account in the numerical simulations. When the frequency is increasing, the value of the refraction angle is decreasing, as expected from the dispersion curve. In the frequency range of interest, there is no index matching between the PC and the epoxy surrounding medium,

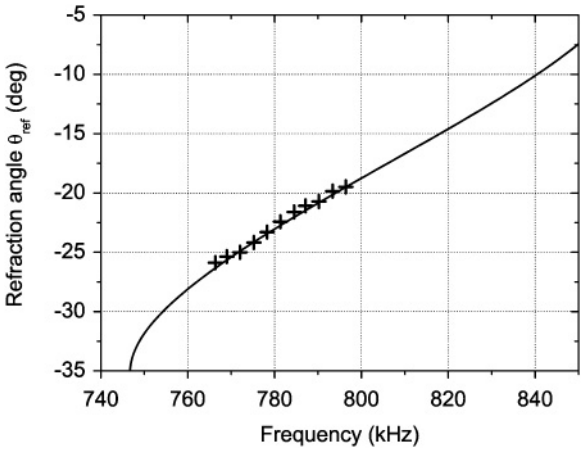

FIG. 6. Variations of the negative angle of refraction as a function of the frequency, measured experimentally (crosses) and computed from the dispersion curves of Fig. 1 (line).

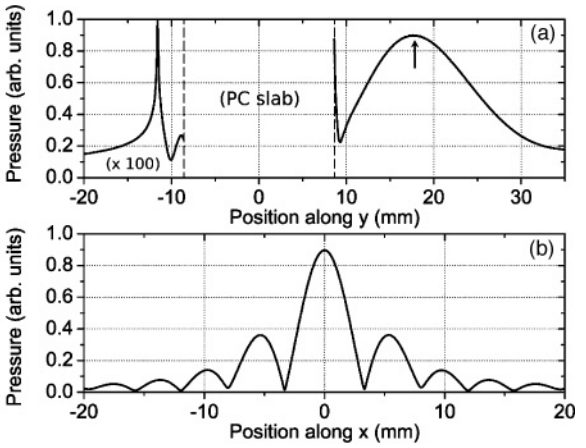

FIG. 8. Plot of the pressure field amplitude (a) along the line perpendicular to the slab that includes the source point and (b) along the line parallel to the slab that includes the focal point, for the simulation of Fig. 7. Here the focal point is defined as the point of maximum amplitude on plot (a) (indicated by an arrow). On (a), the PC slab is situated between the two dashed lines. For clarity, field values on the source side of the slab are divided by 100.

and thus all the exit angles are smaller than 60° and vary between 0° and 35°.

IV. NUMERICAL EXPERIMENT: FLAT LENS IN A FLUID ENVIRONMENT

As stated before, the main advantage of using a longitudinal mode for negative refraction is that the system can be coupled to a surrounding fluid medium. This is an important feature for practical applications in ultrasonic medical imaging devices, involving, for instance, flat lenses.

To check the coupling efficiency, a flat lens based on the PC under study is simulated. The lens is 7 cells thick and 65 cells wide, in order to avoid edge effects. The PC constituting the lens is oriented so that direction ΓX is perpendicular to the interfaces. For this type of simulation, losses in epoxy are taken into account, which allows quantifying more precisely the expected performance of the system. A point pressure source is located 3 mm away from the lower interface, with an excitation frequency of 786 kHz. To obtain a point image for this point source, index matching of the lens with respect to the surrounding fluid must be respected. In other words, the wave number inside and outside the crystal must be the same.[21] For a lens immersed in water, the ratio of the wave numbers $k_{\text{water}}/k_{\text{PC}}$ is ~ -3.8 (which means that, taking water as a refractive index reference, the PC effective index is ~ -0.26).

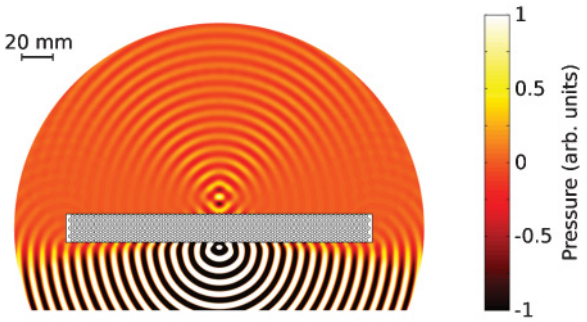

FIG. 7. (Color online) Simulated pressure field (normalized to a source amplitude of 100) for a PC-made flat lens immersed in a fluid, at 786 kHz. The fluid refractive index is matched to the PC index. A point source is located below the lens, 3 mm away from the bottom interface. For clarity, the color scale is cut to ±1 and thus some parts of the field map below the lens are out of the color scale (black and white regions).

For the simulation, a virtual fluid whose index is matched with the PC index (i.e., a fluid with +0.26 refractive index, with respect to water) is used. Figure 7 shows the computed pressure field map. Owing to both the impedance mismatch between the PC and the surrounding fluid and the losses in epoxy, the pressure amplitudes above the slab are ∼100× lower than below it. However, a focusing effect is clearly visible above the flat lens. The focus position is consistent with the theory of flat lenses, because the source-image distance (29.3 mm) is approximately equal to twice the slab thickness (17.22 mm). The full widths at half maximum (FWHM) of the focal spot along the directions perpendicular and parallel to the slab (shown on Fig. 8) are, respectively, 15.19 and 4.18 mm (2.08 λ and 0.57 λ, with λ being the wavelength in the virtual fluid at 786 kHz). Even though optimizing the lens is beyond the scope of this article, it should be noted that the performance in terms of resolution is also affected by the impedance mismatch and the losses. For instance, if a lossless epoxy is considered, the FWHM of the focal spot along the directions perpendicular and parallel to the slab are reduced to 1.51 λ and 0.5 λ, respectively, whereas the source-image distance is increased to 31 mm.

These simulation results demonstrate that the negative refraction effects for longitudinal waves evidenced experimentally can be used to design *solid* flat lenses for imaging systems of *fluid* environments.

V. CONCLUSION

Numerical and experimental evidence of a negative refraction process is reported in the case of longitudinal waves in a solid-solid PC. The PC consists of a triangular array of steel rods embedded in an epoxy matrix. Numerical results, based on the finite-element method coupled to the Snell-Descartes law, are in good agreement with experimental ones. Simulations also show that the solid PC can be effective to image a fluid environment, which is an important issue for applications in medical imaging devices. Future studies will concern index matching, as well as impedance matching, in order to design a flat lens to be used in water.

ACKNOWLEDGMENT

This work is supported by the Agence Nationale de la Recherche: ANR-08-BLAN-0101-01, SUPREME project.

[1] See, for example, the special issue of Z. Kristallogr. **220** (2005), [http://www.oldenbourg-link.com/toc/zkri/220/9-10].

[2] M. Ke, Z. Liu, Z. Cheng, J. Li, P. Peng, and J. Shi, Solid State Commun. **142**, 177 (2007).

[3] W.-P. Yang, L.-Y. Wu, and L.-W. Chen, J. Phys. D **41**, 135408 (2008).

[4] X. Zhang and Z. Liu, Appl. Phys. Lett. **85**, 341 (2004).

[5] M. Farhat, S. Guenneau, S. Enoch, A. B. Movchan, and G. G. Petursson, Appl. Phys. Lett. **96**, 081909 (2010).

[6] J. Li, Z. Liu, and C. Qiu, Phys. Rev. B **73**, 054302 (2006).

[7] S. Yang, J. H. Page, Z. Liu, M. L. Cowan, C. T. Chan, and P. Sheng, Phys. Rev. Lett. **93**, 024301 (2004).

[8] A. Sukhovich, L. J. Jing, and J. H. Page, Phys. Rev. B **77**, 014301 (2008).

[9] Liang Feng, Xiao-Ping Liu, Ming-Hui Lu, Yan-Bin Chen, Yan-Feng Chen, Yi-Wei Mao, Jian Zi, Yong-Yuan Zhu, Shi-Ning Zhu, and Nai-Ben Ming, Phys. Rev. Lett. **96**, 014301 (2006).

[10] J. Bucay, E. Roussel, J. O. Vasseur, P. A. Deymier, A-C. Hladky-Hennion, Y. Pennec, K. Muralidharan, B. Djafari-Rouhani, and B. Dubus, Phys. Rev. B **79**, 214305 (2009).

[11] L.-Y. Wu, W.-P. Yang, and L.-W. Chen, Phys. Lett. A **372**, 2701 (2008).

[12] L.-Y. Wu, L.-W. Chen, and R. C.-C. Wang, Physica B **403**, 3599 (2008).

[13] M. Ke, Z. Liu, C. Qiu, W. Wang, J. Shi, W. Wen, and P. Sheng, Phys. Rev. B **72**, 064306 (2005).

[14] S. Alagoz, O. A. Kaya, and B. B. Alagoz, Appl. Acoust. **70**, 1400 (2009).

[15] A. Sukhovich, B. Merheb, K. Muralidharan, J. O. Vasseur, Y. Pennec, P. A. Deymier, and J. H. Page, Phys. Rev. Lett. **102**, 154301 (2009).

[16] J. Li, Z. Liu, and C. Qiu, Phys. Lett. A **372**, 3861 (2008).

[17] B. Morvan, A. Tinel, A.-C. Hladky-Hennion, J. Vasseur, and B. Dubus., Appl. Phys. Lett. **96**, 101905 (2010).

[18] C.-Y. Chiang and P.-G. Luan, J. Phys.: Condens. Matter **22**, 055405 (2010).

[19] ATILA Finite Element Code for Piezoelectric and Magnetostrictive Transducers Modeling, Version 6.0.0, User's Manual, ISEN, Acoustics Laboratory, Lille, France, 2005.

[20] A.-C. Hladky-Hennion, J. O. Vasseur, B. Dubus, B. Djafari-Rouhani, B. Morvan, A. Tinel, and D. Ekeom, Proceedings of the 2008 IEEE Ultrasonic Symposium., Beijing, China, 253–256 (2008).

[21] V. G. Veselago, Sov. Phys. Usp. **10**, 509 (1968).